Stacking-Sequence Changes and Na Ordering in Layered Intercalation Materials

Julija Vinckevičiūtė,[ID] Maxwell D. Radin, and Anton Van der Ven*

Materials Department, University of California, Santa Barbara, Santa Barbara, California 93106, United States

ABSTRACT: The performance of Na-ion batteries is sensitive to the nature of cation ordering and phase transformations that occur within the intercalation compounds used as electrodes. In order to elucidate these effects in layered Na intercalation compounds, we have carried out a first-principles statistical mechanics study of Na ordering and stacking-sequence preferences in the model compound Na_xTiS_2. Our calculations predict a series of structural phase transitions at room temperature between O3, P3, O1, O1−O3 staged hybrid, and O1−P3 staged hybrid. We further explore the ordering of Na ions in P3 and O3 and find that these host structures favor very distinct Na-vacancy patterns. Low energy orderings on the honeycomb lattice in P3 consist of triangular island domains with vacancies coalescing at antiphase boundaries. This results in a devil's staircase of ground-state Na orderings within P3 that are unlike the orderings possible in the triangular lattice of Na sites in O3. We explore the role that antiphase boundaries play in mediating Na diffusion in the P3 host.
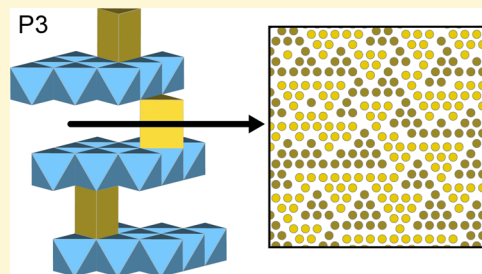
INTRODUCTION

Improvements in electrochemical energy storage are important in promoting renewable energy in transportation and grid storage. Increasing attention has been drawn to Na-ion intercalation materials as an alternative to Li-ion batteries.[1,2] Not only is Na more abundant than Li, but Na-ion electrode materials also behave differently from their Li-ion counterparts due to differences in ionic size and electronic structure. One stark contrast is the stability of prismatic coordination of Na in layered oxides and sulfides, which is not observed in Li due to the latter's smaller ionic radius.[3−6] The crystal structure of the host plays a crucial role in determining electrochemical voltage profiles, cation diffusion mechanisms, and diffusion coefficients.[7] Layered Na intercalation compounds undergo phase transformation sequences that are distinct from those seen in Li-ion electrode materials and as yet not thoroughly explored.[8−22] Such phase transformations can cause degradation as stresses accompanying changes in structure may induce crack initiation and growth.[23,24] Phase transformations can also lead to irreversibilities and hysteresis in the voltage profile due to asymmetries between the multiple kinetic processes required to affect an abrupt change in crystal structure and composition.[25] Phase transformations are generally avoided to increase the lifetime of the battery, which often limits the battery's capacity. It is, therefore, crucial to understand when structural changes occur, how they affect the properties of the battery, and whether they can be suppressed.

A large number of layered Na transition-metal oxides and sulfides has been studied experimentally,[6] and many form the O3 crystal structure[8] when synthesized as $NaMO_2$ or $NaMS_2$ (where M is a transition metal). The size and electronegativity of the anions and cations appears to play a decisive role in determining whether O3 undergoes a stacking-sequence change to a P3 host structure upon Na removal.[3,4,26] For example, the

O3 forms of $NaCoO_2$, $NaNiO_2$, and their alloys undergo a transformation to P3 during deintercalation,[8−10,15,20] while $NaTiO_2$ maintains its O3 host at high levels of charge.[22] In some compounds such as Na_xVO_2, the transition from O3 to P3 requires thermal activation.[27] The large number of steps in the voltage profiles of many layered Na intercalation compounds suggests a prevalence of phase transitions associated with Na ordering and/or stacking-sequence changes.[8,10−12,16−20] The steps are usually more pronounced than in most layered Li-intercalation compounds. Ordering tendencies within the P3 host remain largely unexplored, especially at finite temperature. Diffusion mechanisms within the P3 host are also not fully understood,[28] but experimental evidence for $Na_xCo_{0.6}Ni_{0.4}O_2$ suggests that Na mobility may be higher in P3 than in O3.[10] A common property of many transition-metal oxides and sulfides is the importance of local interactions between the transition metal and Na. Local charge ordering and Jahn−Teller distortions, for example, have been shown to affect ordering preferences among Na within layered intercalation compounds.[29]

In this study, we use the Na_xTiS_2 ($0 < x < 1$) system as a model to study phase stability and intercalating cation ordering in the O1/O3/P3 family of structures using first-principles statistical mechanics approaches. This system has been studied experimentally and found to exhibit O1/O3/P3 family stacking and staging phenomena.[30−32] The absence of localized charge ordering and Jahn−Teller distortions in Na_xTiS_2 makes it an ideal model to isolate the role of Na−Na interactions and host crystal structure on phase stability and Na ordering tendencies.[33,34] We combine first-principles density functional

theory with the cluster expansion formalism and grand canonical Monte Carlo simulations to predict phase stability, finite temperature ordering, and the equilibrium voltage curve at 300 K. We find that the P3 host structure is not only stabilized at intermediate Na concentrations but that hybrid staged structures with mixed O1−O3 and O1−P3 stackings are also stable at low Na concentrations. In addition, we find that the Na ions and vacancies in the P3 host, due to its honeycomb lattice, organize into triangular islands of perfectly ordered domains separated by antiphase boundaries at high Na concentrations. This results in a devil's staircase of ground-state orderings[35,36] that has not been previously explored in layered intercalation materials at finite temperatures. An analysis of migration pathways in P3 suggests that the diffusion mechanisms may be fundamentally different from those in O3, with antiphase boundaries serving as channels for Na transport. Our findings for Na_xTiS_2 shed light on structural stability, ordering tendencies, and diffusion mechanisms in other layered oxide and sulfide materials.

■ STRUCTURE OVERVIEW

Layered sodium transition-metal oxides and sulfides have Na_xMX_2 stoichiometry, where Na is the intercalating sodium species, M stands for transition-metal cations, and X represents sulfur or oxygen anions. The structure is made up of layers of two-dimensional, close-packed triangular lattices occupied by Na, M, or X ions. Following convention, we label the three relative positionings within a triangular lattice with the letters A, B, and C, as illustrated in Figure 1a. Two X anion layers with
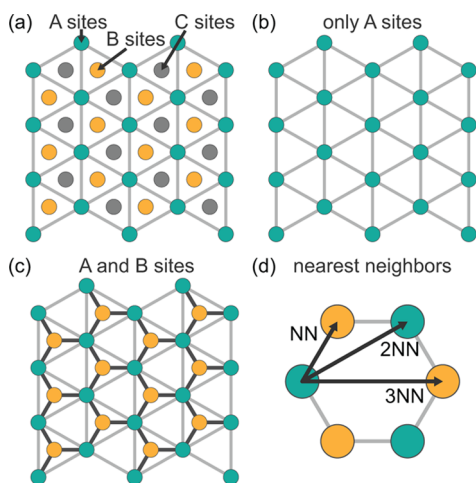

Figure 1. (a) Projection of the three different positionings of a triangular lattice. (b) In O3, the octahedral Na sites form a simple triangular lattice. (c) In P3, the Na ions can occupy one of two symmetrically equivalent trigonal prismatic sites per transition metal that collectively form a honeycomb lattice. (d) First-nearest-neighbor pairs (NN) are much closer in the honeycomb than in the triangular lattice and are unfavorable for simultaneous occupation. The second-nearest-neighbor pairs (2NN) on a honeycomb are the same as the NN of the triangular lattice.

AB stacking surround a layer of M atoms with C positioning, forming MX_2 sheets of edge-sharing M−X octahedra. The interlayer spacing between the octahedral MX_2 sheets allows for Na intercalation, and the stacking of the MX_2 sheets relative to each other determines whether the Na sites are octahedrally (O) or prismatically (P) coordinated by X.

The O1, O3, and P3 hosts (using the notation of Delmas[8]) belong to an important family of related layered Na intercalation compounds. In the O1 host, the X sublattice has *AB*-type stacking (Figure 2a). This results in octahedrally
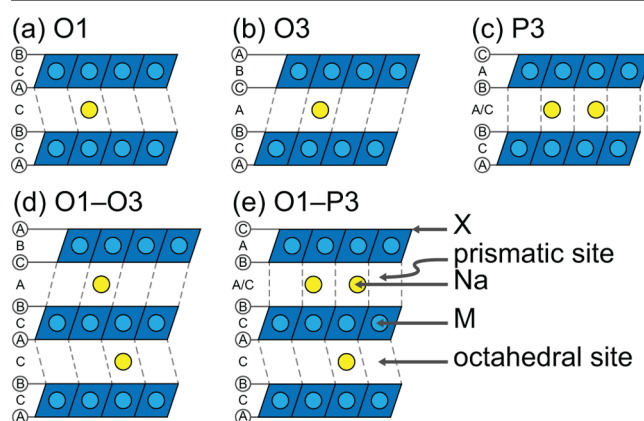

Figure 2. Side-view depiction of relative stackings of MX_2 octahedral sheets that result in (a) O1, (b) O3, and (c) P3 structures as well as hybrids (d) O1−O3 and (e) O1−P3. MX_2 octahedra are depicted as blue parallelograms with M in the center and X at the corners (not explicitly shown). Na ions are yellow circles occupying an octahedral site or one of two symmetrically equivalent prismatic sites. Relative site positions are indicated using A, B, and C, with X positions circled.

coordinated Na sites that share faces with the transition-metal octahedra. The O3 host has an *AB CA BC* anion sublattice stacking sequence and also has octahedrally coordinated Na sites; however, these do not share faces with the transition-metal octahedra (Figure 2b). The P3 host instead exhibits *AB BC CA* stacking, resulting in prismatic sites in the Na layer that each share one face with an M−X octahedron (Figure 2c). The difference between octahedral and prismatic sites is illustrated in Figure 3. Each of these host structures can transform into one of the other without the breaking of M−X bonds through a simple gliding of the MX_2 sheets.
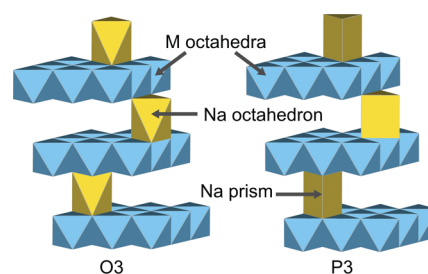

Figure 3. Three-dimensional models of the octahedral Na sites in O3 and the prismatic Na sites in P3. There are two unique prismatic sites in P3. Yellow polyhedra indicate Na sites, blue octahedra depict M sites, and X are not explicitly shown but occupy the corners of the polyhedra.[37]

This structure library can be extended to include a mixture of the pure stacking sequences (Figure 2d,e). Such hybrids may become stable at low intercalant concentrations, as occurs in Li_xCoO_2, where a hybrid combining the stacking sequences of O1 and O3, named H1−3, forms at low Li concentrations.[38,39] In this study, we will refer to the H1−3 hybrid as O1−O3. In addition, we consider a hybrid that combines O1 and P3 hosts. Though Li-ion electrode materials generally do not exhibit P3

stacking due to the small ionic size of Li, the larger size of Na ions stabilize the P3 structure and make an O1−P3 hybrid a likely host of ground-state configurations in Na_xMX_2.

Not only do Na atoms have different X coordination in O1, O3, and P3, but their sites within the Na layer also form different two-dimensional lattices. The Na sites of O1 and O3 form two-dimensional triangular lattices (Figure 1b). In P3, the anion layers on both sides of a Na layer are directly on top of each other (e.g., C C stacking), resulting in two trigonal prismatic sites (A and B) for Na occupation per transition metal (Figure 1c). The combination of all prismatic sites within a particular Na layer of P3 generates a honeycomb lattice. The honeycomb pattern is actually a triangular lattice with a two-atom basis and not strictly a lattice of its own, but we will use the term "honeycomb lattice" to distinguish it from the one-atom basis triangular lattice. Each prismatic Na site of P3 shares a face with one M−X octrahedron directly above or directly below it, depending on the sublattice that it belongs to. This makes the two prismatic sites symmetrically equivalent. The existence of two symmetrically equivalent Na sites per transition metal in P3 results in Na−Na distances not available on the triangular lattices of O3 and O1 (Figure 1d). While two nearest-neighbor sites on the honeycomb lattice within the Na layers will not be simultaneously occupied due to electrostatic and steric interactions (pair labeled NN in Figure 1d), the availability of other new pairs (e.g., 3NN in Figure 1d) allows for Na orderings not possible in a triangular lattice.

■ METHODS

We investigated phase stability of Na_xTiS_2 as a function of Na concentration, x, at zero Kelvin and at room temperature using first-principles statistical mechanics methods. The equilibrium phases at zero Kelvin are those that minimize the energy of the system. Energies of different structures having composition Na_xTiS_2 were calculated with first-principles density functional theory (DFT) using the Vienna Ab Initio Simulation Package[40,41] with PAW pseudopotentials[42,43] and the optB86b-vdW functional.[44−47] Based on convergence tests, the energy cutoff was chosen to be 530 eV and the k-point mesh density 30 Å. See Table 1 for details on number of calculations completed.

Table 1. Details of the Cluster Expansions for the Various Hosts

structure	calculated[a]	clusters in fit[b]	WRMS (meV)[c]	TiS_2 units in MC[d]
O1	15			
O3	193	21	2.1	9600
P3	277	25	2.7	8192
O1−O3	91	17	0.9	5400
O1−P3	60	16	3.9	7776

[a]Number of symmetrically distinct Na-vacancy orderings that converged and did not relax to a different structure during DFT energy minimization. [b]Number of non-zero expansion coefficients in the cluster expansion. [c]Weighted RMS error per formula unit, which indicates how well the CEs fit the DFT data. [d]Number of Na_xTiS_2 unit cells in supercells used in the MC simulation.

Equilibrium at finite temperature is determined by a minimum of the free energy, which has contributions from entropy arising from thermal excitations. Layered Na transition-metal intercalation compounds are stable in a variety of host crystal structures depending on their Na concentration and temperature. Since the candidate host structures have distinct symmetries, they can each be described thermodynamically by a separate free energy. Configurational degrees of freedom resulting from all the possible ways of distributing Na and vacancies over intercalation sites are the dominant source of entropy for intercalation compounds at room temperature.[48] We calculated free energies as a function of composition and temperature for the O3, the P3, the O1−O3 hybrid (i.e., H1−3), and the O1−P3 hybrid host structures with a cluster expansion (CE) approach and grand canonical Monte Carlo (MC) simulations. A cluster expansion,[49,50] parametrized with first-principles DFT-based calculations, enables a rapid calculation of the energy of individual Na-vacancy orderings. This makes it possible to calculate thermodynamic averages in MC simulations.

The Clusters Approach to Statistical Mechanics (CASM)[51−54] software package was used to construct a CE for each host structure (except for O1) and to perform grand canonical MC simulations. A large number of Na-vacancy orderings were enumerated within each host structure. The fully relaxed energies of these orderings were calculated with DFT (optB86b-vdW) and were used to parametrize the expansion coefficients of each CE via a genetic algorithm.[55] In the present study, the clusters of each CE were limited to points, pairs, triplets, and quadruplets. The weighted root-mean-square (WRMS) (Table 1) was less than 4 meV in each CE, where the weights were assigned exponentially with respect to the distance from the local convex hull. Grand canonical MC simulations were applied to each CE to calculate the dependence of the Na concentration on chemical potential and temperature (supercell sizes for MC simulations are listed in Table 1). These relationships were integrated to calculate free energies for each host structure.[56] A grid of chemical potentials with increments of no more than 25 meV/atom was used at different temperatures. Cooling runs were performed for each chemical potential from 1000 to 100 K at a 5 K interval.

The voltage of a Na battery is related to the difference in Na chemical potential between the cathode and the anode according to

$$V = -\frac{\mu_{Na} - \mu_{Na}^0}{e}$$

where μ_{Na} is the chemical potential of Na in the cathode, μ_{Na}^0 is the Na chemical potential of the reference anode (which we chose as metallic Na), and e is the elementary charge.

As will be expanded on below, our DFT results predict that the O1 structure is only stable at composition x = 0. This is observed in many other intercalation materials, including Li_xCoO_2.[38] Since there are no Na atoms to generate configurational entropy at this composition, we set the free energy of O1 equal to its energy. Likewise, the O1 layers in the O1−P3 and O1−O3 hybrids were assumed to remain vacant in the entire Na composition range. This results in staging, wherein every other Na layer is left completely unoccupied.

■ RESULTS

Zero Temperature. Figure 4 shows the DFT formation energies of the ground-state Na-vacancy orderings within each host structure. The formation energies in Figure 4 are calculated relative to O1 TiS_2 at x = 0 and O3 $NaTiS_2$ at x = 1. The ground-state orderings were determined by finding the convex hull of the fully relaxed energies of all Na-vacancy orderings considered within the different hosts. While the energies of a large number of Na-vacancy orderings were calculated (Table 1), there may be lower energy orderings in large supercells that were not considered in this study. This is especially true for the P3 host since previous studies of low-energy orderings on the honeycomb lattice using short-range lattice model Hamiltonians[35] have predicted a sequence of ground state orderings requiring supercells that are substantially larger than can be treated with current DFT methods.

The global convex hull of all orderings (solid black line in Figure 4) shows that the relative stability among the different hosts is very sensitive to Na concentration. At high Na concentrations ($7/8 \leq x \leq 1$), O3 is predicted to be stable. The P3 host becomes stable at intermediate Na concentrations ($1/2 < x < 3/4$), with a small two-phase region ($3/4 < x < 7/8$)
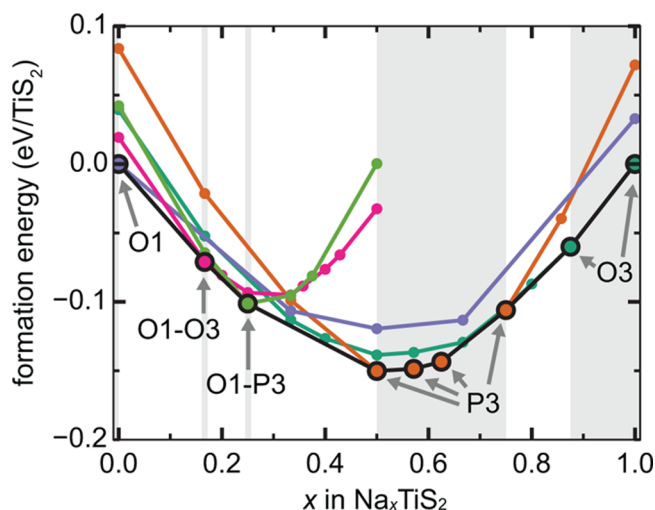
Figure 4. Calculated formation energies of configurations on the convex hull for each host structure. Configurations with energies above the hull are not shown. The global convex hull is outlined in black.

separating O3 from P3, consistent with experimental studies that observe P3 stacking in deintercalated Na_xTiS_2.[19,57] Below $x = 1/2$, the hybrid phases O1–P3 and O1–O3 are stable with ground state orderings at $x = 1/4$ and $x = 1/6$, respectively. In these structures, the O1 layers are empty, and the lowest energy configurations of the P3 and O3 layers are similar to those on the hulls of their respective nonhybrid structures. Finally, at $x = 0$, the O1 host becomes stable.

It is instructive to inspect the low-energy Na-vacancy orderings in the P3 host and compare them to orderings in O3. At $x = 1$, there is only one Na configuration possible in O3

as all sites of its triangular lattices are occupied at this composition. In P3, the lowest energy ordering at $x = 1$ has Na occupying exclusively one of the triangular sublattices as shown in Figure 5a. Any other ordering in P3 at this composition would require the simultaneous occupation of a nearest-neighbor pair, which would lead to a very large energy penalty due to strong electrostatic and steric repulsion through the shared face of a pair of nearest-neighbor trigonal prismatic sites.

Below the composition of $x = 1$, vacancies are incorporated differently in P3 than in O3. In O3, which has a single triangular lattice, any ordering can be achieved by simply removing Na atoms. Although this mechanism can occur in P3, it is more favorable to remove Na atoms while rearranging others to occupy a mixture of the two available sublattices in a honeycomb lattice. This can result in domains that consist of Na atoms that occupy a single triangular sublattice as at $x = 1$. These domains are separated by antiphase boundaries (APBs), which accommodate the vacancies that are introduced as Na is extracted. For instance, the lowest-energy ordering enumerated in P3 at $x = 6/7$ (Figure 5b) consists of alternating, linear strips of A domains and B domains (two colors are used to highlight the difference in sublattice occupation). APBs separate the strips and concentrate the vacancies introduced upon removal of Na. This leads to a reduction in energy as the APBs allow an increase in the distance between neighboring Na ions. The ground states at $x = 3/4$, $5/8$, and $4/7$ (Figure 5c–e) accommodate vacancies in a similar way. The total length of APBs must increase as the vacancy concentration increases (Na concentration decreases). This is achieved by reducing the size of A and B domains. The orderings at $x = 5/8$ and $x = 4/7$ consist of isolated two-atom and three-atom islands as can be seen in Figure 5d,e.
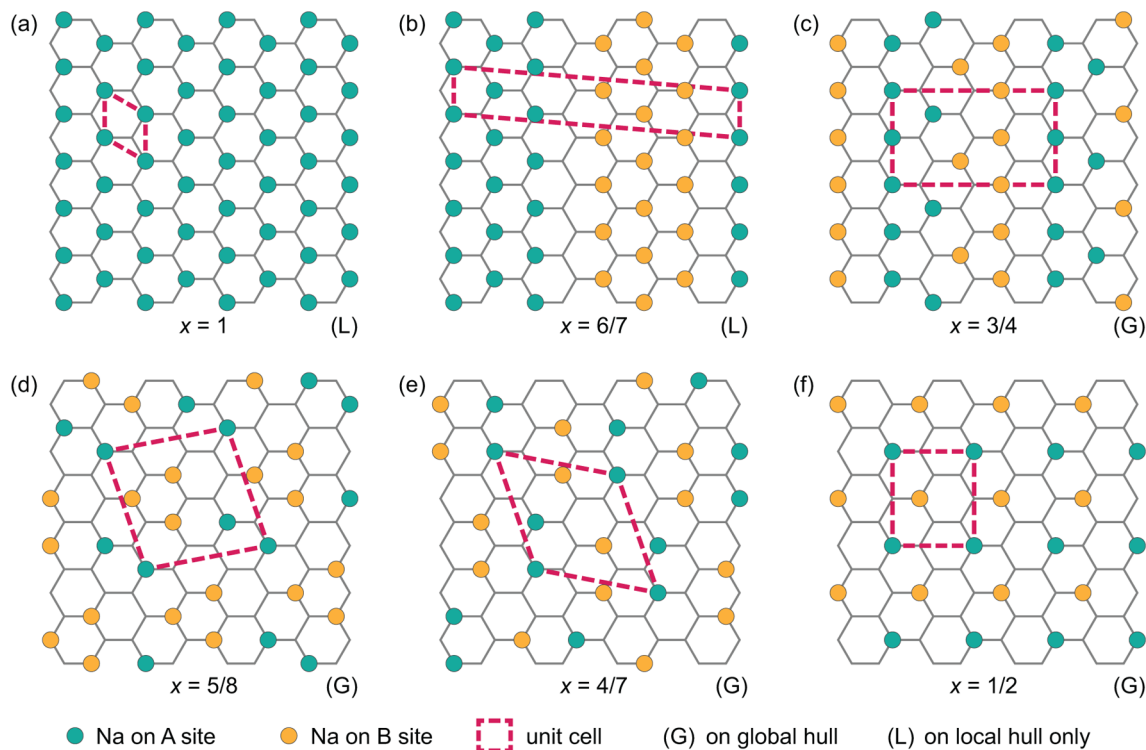

Figure 5. Na-vacancy orderings on the convex hull of enumerated configurations within P3. Occupancy of the two sublattices on the honeycomb lattice of P3 is distinguished with different colors (green and yellow).

The low-energy orderings in P3 shown in Figure 5a−e are consistent with past studies of ground state orderings on the honeycomb lattice. Using simple lattice model Hamiltonians, Kanamori[35] showed that repulsive nearest- and second-nearest-neighbor pair interactions on the honeycomb lattice result in a devil's staircase of a countably infinite number of ground state orderings consisting of APBs. The devil's staircase starts with full occupancy on one sublattice as in Figure 5a and continues with orderings having triangular A and B island-like domains separated by APBs, such as the ordering illustrated in Figure 6.
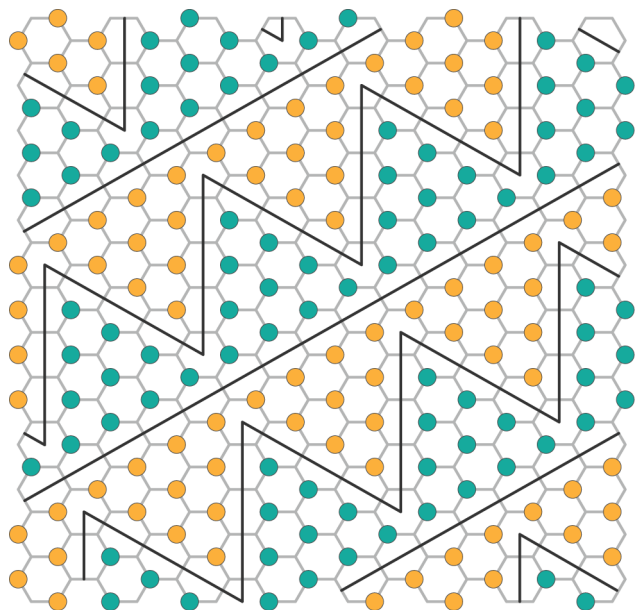

Figure 6. Example of a ground state ordering on a honeycomb lattice belonging to the devil's staircase discovered by Kanamori.[35] Occupancy of the two sublattices on the honeycomb lattice is distinguished by use of green and yellow circles. Triangular island-like domains are separated by antiphase boundaries (black lines).

The A and B domains correspond to perfectly ordered regions with Na occupying exclusively one sublattice. The APBs that separate the domains are indicated by solid black lines. Such large triangular islands are not present in enumerated orderings calculated using DFT as these orderings require large supercells.

At $x = 1/2$, the lowest energy ordering in the P3 host does not consist of domains separated by APBs; instead, Na atoms uniformly distribute themselves over the two available sublattices of the honeycomb (Figure 5f). This configuration

is compared to $x = 1/2$ orderings in the O3 host in Figure 7. We found two nearly degenerate, low-energy orderings for O3 at $x = 1/2$. One, shown in Figure 7a, is the zigzag line ordering that is a common ground state in Na transition-metal oxides having the O3 structure.[58] The second ordering (Figure 7b), which is the ground state of O3 at $x = 1/2$, consists of clusters of four Na atoms and is less than 1 meV/atom more stable than the zigzag ordering of Figure 7a. A comparison of the low energy O3 orderings of Figure 7a,b with the $x = 1/2$ ground state in P3 (Figure 7c) reveals that the Na ions in P3 have more flexibility as to how they can order due to the availability of two triangular sublattices. While nearest neighbors cannot be avoided in the O3 structure at this composition, the additional available sites on the honeycomb of the P3 host enable Na atoms to be spaced farther apart from each other. This ability to increase the distance between neighboring Na ions within P3 relative to O3 is likely a dominant factor making P3 more stable than O3 at intermediate Na concentrations, despite the unfavorable face-sharing repulsive interactions between prismatic Na sites and the TiS$_2$ octahedra in P3.

Finite Temperature. First-principles DFT energies of different Na-vacancy orderings were used to parametrize cluster expansions for each host, which were subsequently subjected to grand canonical Monte Carlo (MC) simulations to calculate finite-temperature thermodynamic properties. Figure 8a shows the calculated free energy curves as a function of Na concentration at 300 K for the different host structures. Application of the common-tangent construction reveals that all of the stacking sequences that were on the DFT global hull are still stable at 300 K, starting with O1 at $x = 0$ and continuing to O1−O3, O1−P3, P3, and O3 upon Na intercalation. At temperatures slightly above 300 K, the O1−O3 phase is no longer stable relative to O1 and O1−P3. The MC simulations predict that most ground-state orderings undergo an order−disorder transition below room temperature. One exception is the ground state ordering at $x = 1/2$ in P3. It is predicted to disorder slightly above room temperature.

Figure 8b shows the predicted voltage curve at 300 K, which is related to the slope of the free energy curves in Figure 8a. Sloping regions in voltage signify single phase regions, while plateaus, which arise from a constant chemical potential along a common tangent, indicate a coexistence between two phases. The predicted voltage curve also exhibits a small step at $x = 1/2$ due to the stability of Na ordering at that composition at 300 K. The O1−P3 hybrid phase appears as a large step, while O1−O3 is predicted to be stable in a very narrow voltage window. Our results align closely with the features observed experimentally.[19,30−32] These experiments show a region at high Na
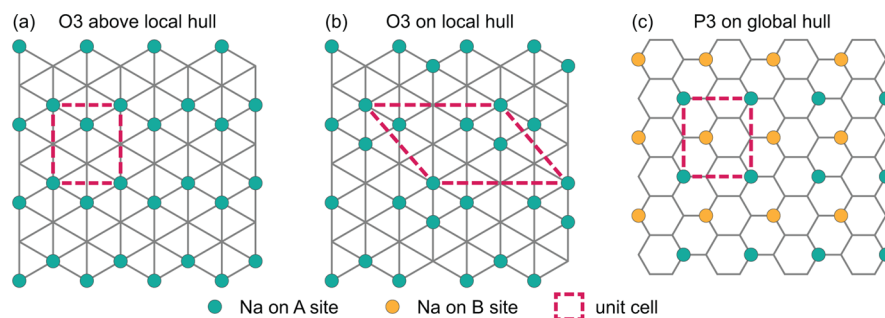

Figure 7. Comparing (a,b) O3 and (c) P3 orderings at $x = 1/2$ shows that, while nearest-neighbor pairs cannot be avoided in O3, the 3NN sites on the honeycomb lattice allow the Na atoms to be more spread out.
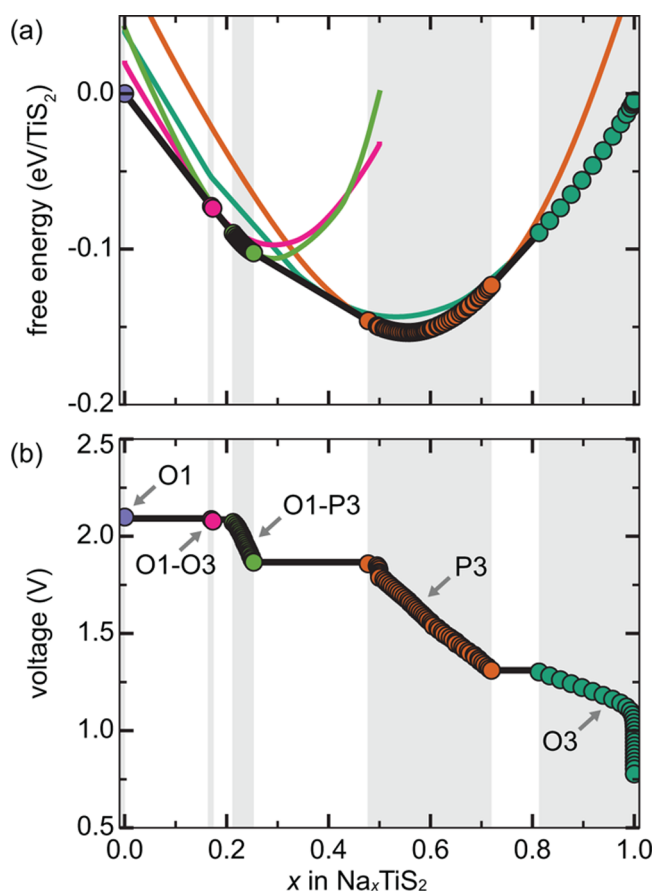
Figure 8. (a) Calculated free energy and (b) equilibrium voltage curve at 300 K. Each host structure (i.e., O3, P3, P3−O1, O3−O1, and O1) has a separate free energy curve. A common tangent construction (black solid line) determines global equilibrium. Gray background indicates single-phase regions, white background is used for two-phase regions.

concentrations of octahedral coordination, a first-order phase transformation to prismatic coordination around $x = 0.8$, and transformations to staged phases at lower Na compositions. In addition to the stage-two ordering that is seen in our calculated voltage curve associated with O1−P3, there is also experimental evidence for a stage-three ordering wherein only every third layer contains Na atoms.[32] Higher-order hybrids (e.g., orderings with O1−O1−P3 layer repeat unit) were not included in our analysis. The sharp step at $x = 0.5$ in the calculated voltage curve, which is due to Na ordering, is shifted to a slightly lower concentration in the voltage curve measured by Winn et al.[31] but to a higher concentration in the voltage curve measured by Lee et al.[19] The shifts may be due to experimental uncertainty in the state of charge.[59]

Microstates from MC simulations of P3 illustrate the importance of APBs even at elevated temperature. Figure 9 shows selected Na layers from several MC sampled microstates for a range of Na concentrations. Different colors are used to distinguish occupancy of the two triangular sublattices of the honeycomb lattice. At $x \approx 1$, Na orders on a single sublattice consistent with the zero Kelvin ground state predicted by DFT. Vacancies at lower Na concentrations are accommodated through the formation of APBs that separate A and B domains. Due to the finite size of the MC supercells and finite chemical potential grid, APBs first appeared around $x = 0.96$. At this Na concentration, the domains are large and triangular, with well-

defined APBs separating extensive A and B domains. As the Na concentration decreases further, more APBs must form, and the domains become smaller. While triangular domains are still easily discernible in Figure 9 in the microstates sampled at $x = 0.9$ and $x = 0.8$, more disorder is observed as the Na concentration approaches $x = 0.7$. Triangular domains are still distinguishable around $x = 0.7$, but there are also many linear chains of Na occupying the same sublattice (A or B). Short-range order persists at $x = 0.6$, although at this concentration short chains of A or B sublattice occupation seem to be preferred. The Na ions order in their zero Kelvin ground state pattern at $x = 0.5$ exhibiting occasional defects due to thermal excitations. They disorder at temperatures slightly above that of room temperature. The in-plane Na ordering at $x = 0.5$ (Figure 5f) is also stable in the P3 layers of O1−P3 at $x = 0.25$ and matches the ordering inferred from single-crystal diffraction data by Hibma.[32] Hibma also reports on the existence of diffraction superlattice spots together with rings above $x = 0.5$. Our MC simulations do not predict long-range ordering at room temperature above $x = 0.5$.

The MC snapshots of Figure 9 illustrate that Na extraction from P3 occurs very differently from other host structures such as O3 and O1. A sloping voltage profile usually signifies a solid solution characterized by uniform disorder among cations and vacancies. In contrast, the sloping voltage profile of P3 is produced by Na arrangements consisting of ordered nanosized domains separated by APBs, where changes in Na concentration lead to an overall increase in total APB length. Figure 8b shows that the voltage profile of the P3 phase is steeper than that of O3. This qualitative behavior is similar to that exhibited by many other layered Na intercalation compounds with O3/P3 transformations.[9−11,16,20]

DISCUSSION

Our first-principles study shows that intercalation in Na$_x$TiS$_2$ is very different from that in the traditional Li-ion battery materials in at least two ways. First, stacking-sequence changes are much more prevalent in Na$_x$TiS$_2$ due to the stability of P3 and its hybrids at intermediate compositions. Second, the devil's staircase of triangular domains on the Na honeycomb lattice of P3 is fundamentally unlike the types of orderings seen in Li layered oxides.

We hypothesize that the behavior of Na$_x$TiS$_2$ may be representative of many other intercalated layered oxides and sulfides. This is supported by the observation of transformations from O3 to P3 upon desodiation in a wide range of compounds, including Na$_x$VS$_2$,[19,60] Na$_x$CoO$_2$,[9,15] Na$_x$NiO$_2$,[20] Na$_x$Ni$_{0.5}$Mn$_{0.5}$O$_2$,[11,13] Na$_x$CrO$_2$,[9,11,16] Na$_x$Mn$_{1−y}$Fe$_y$O$_2$,[14] and Na$_x$Fe$_{0.5}$Co$_{0.5}$O$_2$.[15] Furthermore, many Na compounds (e.g., Na$_x$CoO$_2$, Na$_x$CrO$_2$, and Na$_x$VS$_2$) exhibit voltage curves strikingly similar to that predicted for Na$_x$TiS$_2$. The general pattern seems to be as follows:

1. As deintercalation begins, the voltage curve exhibits a relatively flat region around $0.7 < x < 1$ associated with the deintercalation of O3 and transformation to P3.

2. The $0.4 < x < 0.7$ composition range is typically a P3 single-phase region that exhibits a steep slope. The steepness of the slope is a consequence of the high curvature of the P3 free energy, as can be seen in Figure 8a. The high curvature can be attributed to the strong stabilization of the honeycomb lattice at intermediate concentrations.
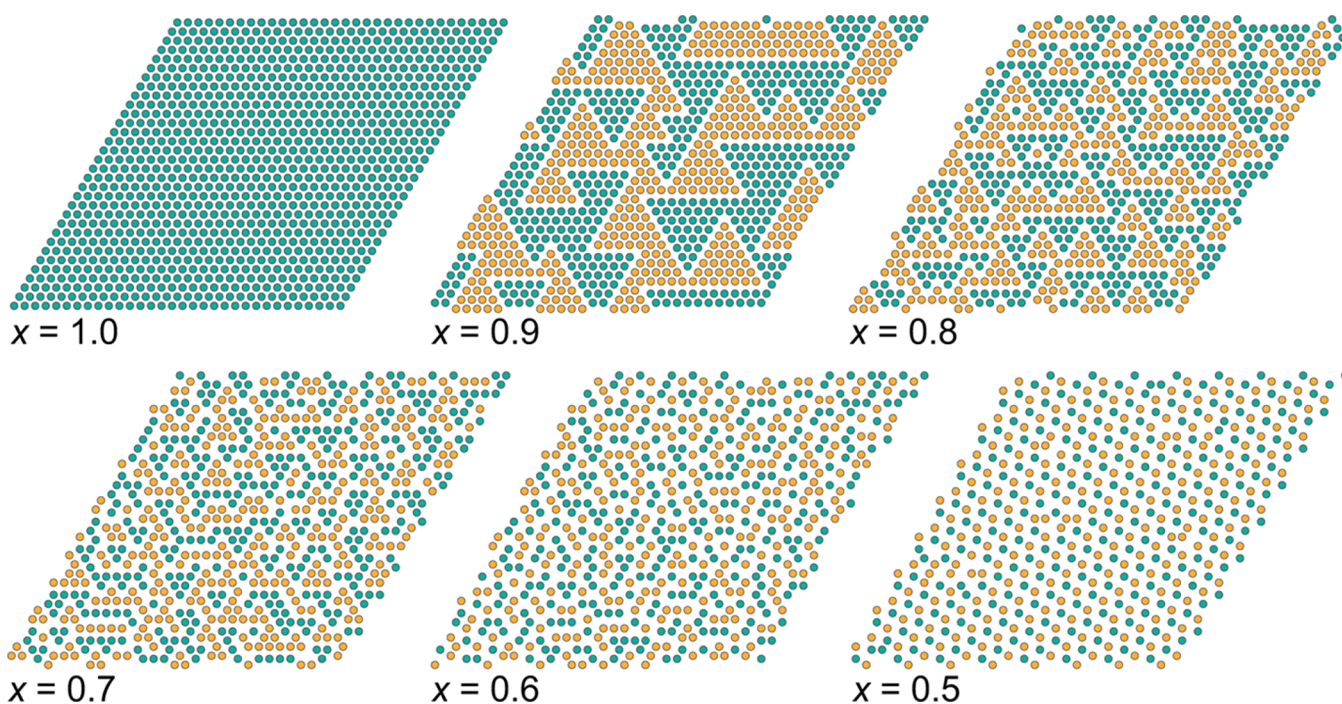
Figure 9. Snapshots from constant chemical potential, decreasing temperature grand canonical Monte Carlo runs for the P3 structure at 300 K, looking down on one of the Na layers. The two different available sites on the honeycomb lattice are shown in green and yellow. Approximate Na concentration at each snapshot is indicated below the snapshot.

3. Around $x = 0.5$, a sharp voltage step occurs, possibly corresponding to a zigzag ordering like that shown in Figure 5f. (This step is often reported at Na contents somewhat above $x = 0.5$, which may be due to the experimental uncertainties in estimating the Na content or the thermodynamic stability of another ordering having a slightly higher Na concentration.[59])

4. Deintercalation beyond $x = 0.5$ exhibits a plateau associated with the transformation of P3 to another stacking sequence. While we are not aware of any experimental observations of staged O1−P3 hybrids at high states of charge in oxides, the results of this study suggest that their occurrence in Na transition-metal oxides could be a possibility at low Na concentrations when the P3 host is also stable at intermediate Na concentrations. Furthermore, stacking sequences at very low Na concentrations may include higher-ordered staged phases as suggested by experiments on Na_xTiS_2.[30,32]

Although many of these materials exhibit additional phase transformations associated with Na/vacancy ordering, the similarities in the structural transformations and overall shape of the voltage curve suggest that these materials share the same basic intercalation physics as Na_xTiS_2. Furthermore, although Li and Mg are unstable in prismatic coordination due to their small ionic sizes, larger intercalating ions such as K^+ and Ca^{2+} may behave similarly to Na in layered compounds. Nevertheless, some Na oxides do not transform to P3 even when their equivalent sulfides are stable in the P3 host. For instance, $NaTiO_2$ is more stable in O3 than P3 even upon deintercalation.[22] This may be a result of increased ionicity in oxides due to higher electronegativity of oxygen versus sulfur.[4,61]

Transformations between O1, O3, P3, and hybrid phases requires stacking-sequence changes during cycling and likely affects battery performance. As was pointed out by Gabrisch et al.,[62] partial dislocations are one mechanism to mediate stacking-sequence changes in layered intercalation compounds. Stresses generated by an array of partial dislocations and by a lattice mismatch across interfaces can contribute to fracture and mechanical degradation. Hybrid phases that nucleate separately and grow into each other may be misaligned, leading to additional sources of stress at their interface.

The honeycomb lattice of Na sites within P3 leads to several interesting properties. At high Na concentration, narrow bands of A and B domains appear in the P3 ground-state orderings calculated with DFT (Figure 5g,h). We can distinguish between three unique Na coordination environments along the APBs in these orderings. Type I APB, shown in Figure 10a, consists of third-nearest-neighbor Na pairs perpendicular to the APB. The APBs that make up the edges of the triangular domains in the MC simulations are type I. Triangles are formed because this type of APB has three symmetrically equivalent orientations. Type II APBs are made up of fourth-nearest-neighbor pairs
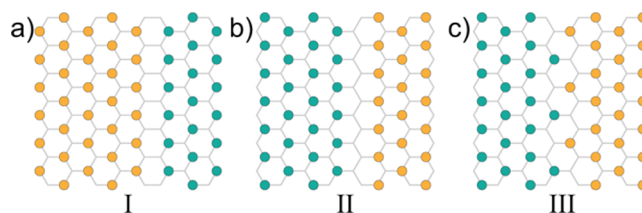

Figure 10. Different types of Na coordination observed along APBs in low-energy orderings found using DFT. (a) Type I ordering is observed along APBs in MC simulations. (b) Type II ordering is not observed in MC simulations. (c) Type III ordering is similar to that observed at corners of triangular domains in MC simulations.
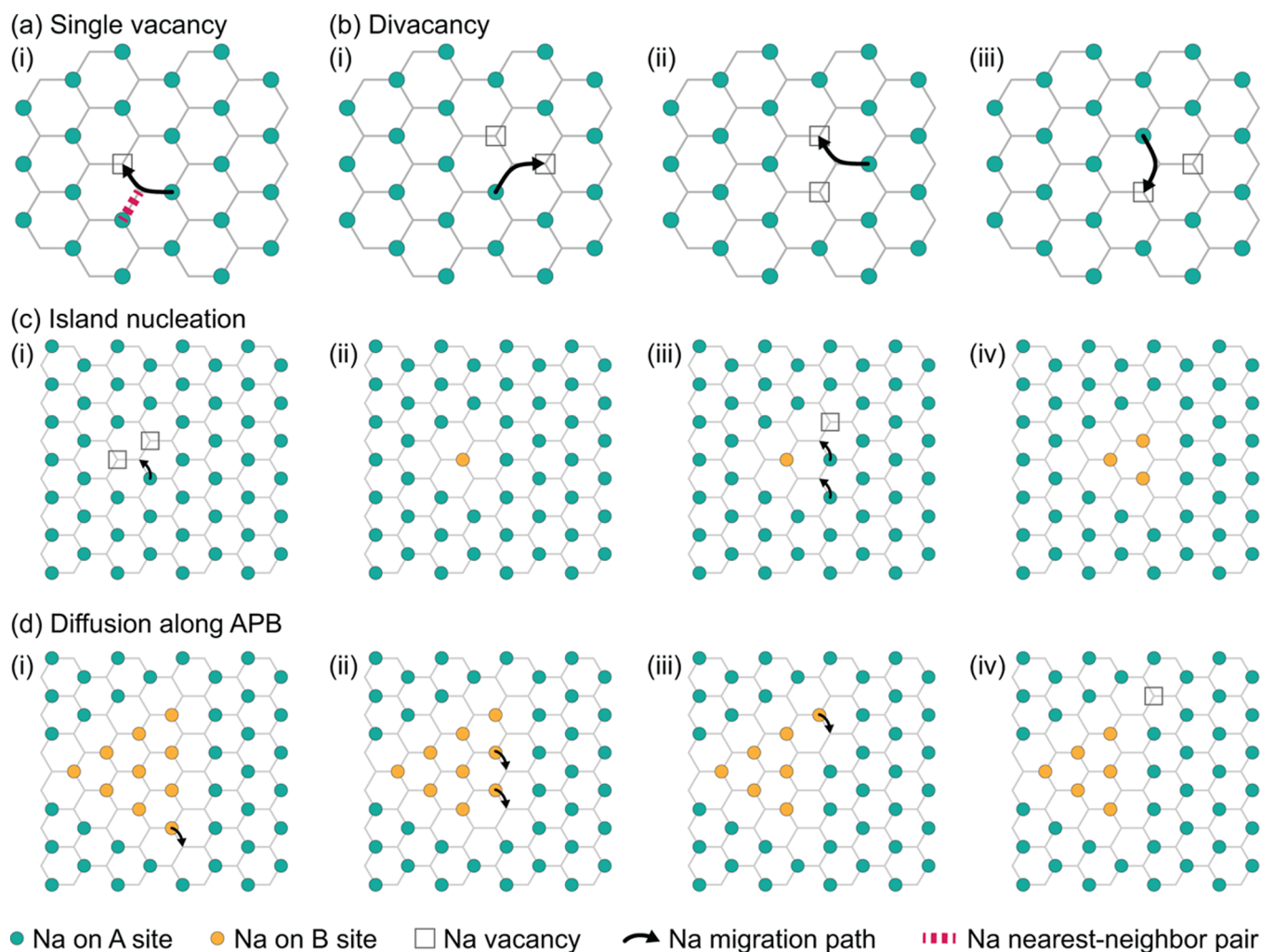
Figure 11. Various migration mechanisms of Na within the P3 host. (a) With an isolated vacancy, an atom must pass through an adjacent trigonal prismatic site that is next to an occupied Na site leading to an unfavorable nearest-neighbor Na−Na repulsive interaction. (b) A divacancy allows for one atom to hop around an axis, but it cannot migrate over an extended distance without invoking high-barrier hops through sites that have an occupied nearest neighbor. (c) A divacancy can aid in new island nucleation, and the island can then easily grow by absorbing isolated vacancies from the surrounding single domain region. (d) Domains can redistribute atoms by shifting antiphase boundaries. This mechanism generates (i → ii → iii → iv) or consumes (iv → iii → ii → i) a vacancy.

(Figure 10b), but this type of boundary is not seen in MC snapshots and is therefore not thermodynamically favorable. When every other atom along a type II APB hops across the boundary, a type III APB forms (Figure 10c). The local Na environment along a type III APB is similar to that observed at corners of triangular domains in MC snapshots.

Others have studied ground states of the devil's staircase on a honeycomb. Kanamori used a simple lattice model Hamiltonian and discovered an infinite series of ground states on a honeycomb lattice with repulsive pairwise interactions.[35] More recently, Wang et al.[36] used a short-range pair Hamiltonian to describe ground states in Na_xCoO_2, where they suggest two different patterns for arranging the triangular domains. Our MC snapshots most closely match the T series suggested by Kanamori. In all of these cases, however, only type I APBs are predicted as separating perfectly ordered domains.

Diffusion mechanisms in the P3 host are qualitatively different from those in other layered intercalation compounds. While the O3 and O1 hosts have a network of interconnected octahedral and tetrahedral sites within the intercalation layer, the P3 host only provides trigonal prismatic sites. A cation in

O3 or O1 migrates between two adjacent octahedral sites by passing through an intermediate tetrahedral site.[7] In P3, cations hopping between nearest-neighbor sites on the same triangular sublattice of the honeycomb lattice (e.g., nearest-neighbor pairs on the A sublattice) will pass through a nearest neighbor prismatic site on the other sublattice (i.e., the B sublattice)[28] as illustrated in Figure 11a.

Vacancies are crucial in facilitating ionic transport in layered intercalation compounds. In fact, in many intercalation compounds, both the qualitative nature of the hop mechanism and the hop rate itself are very sensitive to the local concentration and arrangement of vacancies.[7] A Na ion that migrates into an isolated vacancy within a single-domain region within P3 must pass through the intermediate prismatic site that shares a face with another occupied prismatic site, as illustrated in Figure 11a. This leads to a high-energy nearest-neighbor repulsion along the hop path, making single vacancy hops less favorable than hops in local environments where such nearest-neighbor Na−Na interactions can be avoided.

Unlike in the O1 and O3 hosts, where divacancies are essential for fast diffusion, the presence of a pair of vacancies

within perfectly ordered triangular islands in P3 is unlikely to be much more effective than isolated vacancies in mediating long-range Na diffusion. As illustrated in Figure 11b, a divacancy on a honeycomb lattice is essentially pinned spatially and requires single-vacancy-type hops involving nearest-neighbor Na–Na interactions to redistribute Na ions over long distances. Due to the topology of the honeycomb lattice, only one Na can hop into a divacancy without passing through a site that involves a Na–Na nearest-neighbor interaction (Figure 11b(i)). Upon completion of this hop, only that same Na can perform a subsequent hop that does not involve a Na–Na nearest-neighbor interaction. It has two options then. It can either migrate to the second vacancy (as illustrated in Figure 11b(ii)) or it can hop back to its initial position. If limited to migration paths that avoid nearest-neighbor Na–Na interactions, the divacancy twirls around a single axis without mediating long-range transport of the migrating Na. It is only after another Na performs a hop that requires a nearest-neighbor Na–Na interaction, similar to that encountered in an isolated vacancy hop, that the divacancy can break away and spatially move.

It must be noted, though, that it is very unlikely that divacancies are long-lived within a single domain region as they can facilitate the nucleation of new islands within a single domain region. This is illustrated in Figure 11c. At least two vacancies are required for a Na atom to move from an A site to a B site in a single-domain A region without producing nearest-neighbor pairs. Once initiated, a single point vacancy can be used to grow the B domain at the expense of shrinking the A domain and increasing the total length of APBs.

While Na hops in single-domain regions of P3 generally require passage through high energy sites that involve nearest-neighbor Na interactions, diffusion along APBs can avoid such sites. One possible diffusion mechanism along a domain edge is illustrated in Figure 11d. When no point vacancies are present, Na at the corner of a triangular island can easily migrate onto the other sublattice, allowing the subsequent Na atoms along the APB to migrate across the APB. One domain region then grows at the expense of the other and the total length of APBs decreases. This results in a point vacancy forming within a single-domain region to retain the same overall Na concentration (Figure 11d(iv)).

At this point, the vacancy can take one of three paths. It can move back along the APB in a chain of low-energy steps to reverse the process (the reverse of the process that is illustrated in Figure 11d). Alternatively, a single high-barrier hop would be required to move the vacancy around the corner of the perfectly ordered domain such that it can propagate along an adjacent APB on the same island. Lastly, the vacancy can migrate through a single-domain region via a series of high-energy hops to reach the edge or corner of another APB. Diffusion of the vacancy through a single-domain region may be slow if the domains are large. In all cases, the point vacancy at a corner or an edge of a triangle can quickly travel along the APB and be consumed as the total length of APBs increases. In this way, triangle islands can shrink and expand, and APBs can serve as sources and sinks for vacancies.

As the Monte Carlo microstates illustrate in Figure 9, a decrease in the Na concentration within P3 results in the elongation of the total APB length, which is achieved by an increase in the number of single domain islands. The removal of Na therefore requires the nucleation of new islands and a decrease in the size of the existing islands. These are highly nonlocal readjustments to the overall Na arrangement. It is,

therefore, likely that metastable states that are kinetically more expedient are frequently accessed, especially during high rates of charge and discharge. This could lead to path hysteresis and polarization in the voltage profile; however, a kinetic study involving kinetic Monte Carlo would be necessary to elucidate these tendencies.

CONCLUSION

In this study, we used a first-principles statistical mechanics approach to examine two properties of the O1/O3/P3 family of Na-ion electrode materials: (i) the relative stability among different stacking sequences that include staged hybrid host structures and (ii) Na ordering tendencies in the P3 host. Using Na_xTiS_2 as a model system, we found that O1–O3 and O1–P3 hybrid structures are both stable at low Na concentration. The stability of these staged phases in Na_xTiS_2 suggests that they are likely to occur in other layered Na oxide and sulfide intercalation compounds, with important consequences for cyclability and charge/discharge rate capability. Our study also showed that ordering on the honeycomb in P3 not only allows this phase to be more stable than O3 at Na concentrations around $x = 1/2$ but also results in a devil's staircase of ground states at high Na concentrations (including regions where P3 is stable). These ground states consist of perfectly ordered triangular islands separated by antiphase boundaries. Elementary considerations show that the antiphase boundaries may play a crucial role in mediating long-range Na diffusion within the P3 host.

AUTHOR INFORMATION

Corresponding Author
*E-mail: avdv@engineering.ucsb.edu.
ORCID ⊙
Julija Vinckevičiūtė: 0000-0002-9921-9605
Notes
The authors declare no competing financial interest.

REFERENCES

(1) Han, M. H.; Gonzalo, E.; Singh, G.; Rojo, T. A Comprehensive Review of Sodium layered Oxides: Powerful Cathodes for Na-Ion Batteries. *Energy Environ. Sci.* **2015**, *8*, 81−102.
(2) Kundu, D.; Talaie, E.; Duffort, V.; Nazar, L. F. The Emerging Chemistry of Sodium Ion Batteries for Electrochemical Energy Storage. *Angew. Chem., Int. Ed.* **2015**, *54*, 3431−3448.
(3) Delmas, C.; Fouassier, C.; Hagenmuller, P. Stabilite Relative des Environnements Octaedrique et Prismatique Triangulaire dans les Oxydes Lamellaires Alcalins A$_x$MO$_2$ ($x \leq 1$). *Mater. Res. Bull.* **1976**, *11*, 1483−1488.

(4) Rouxel, J. Sur un Diagramme Ionicité-Structure pour les Composes Intercalaires Alcalins des Sulfures Lamellaires. *J. Solid State Chem.* **1976**, *17*, 223−229.

(5) Whittingham, M. S. Lithium Batteries and Cathode Materials. *Chem. Rev.* **2004**, *104*, 4271−4301.

(6) Yabuuchi, N.; Kubota, K.; Dahbi, M.; Komaba, S. Research Development on Sodium-Ion Batteries. *Chem. Rev.* **2014**, *114*, 11636−11682.

(7) Van der Ven, A.; Bhattacharya, J.; Belak, A. A. Understanding Li Diffusion in Li-Intercalation Compounds. *Acc. Chem. Res.* **2013**, *46*, 1216−1225.

(8) Delmas, C.; Braconnier, J.; Fouassier, C.; Hagenmuller, P. Electrochemical Intercalation of Sodium in Na_xCoO_2 Bronzes. *Solid State Ionics* **1981**, *3−4*, 165−169.

(9) Miyazaki, S.; Kikkawa, S.; Koizumi, M. Chemical and Electrochemical Deintercalations of the Layered Compounds $LiMO_2$ (M = Cr, Co) and $NaM'O_2$ (M' = Cr, Fe, Co, Ni). *Synth. Met.* **1983**, *6*, 211−217.

(10) Saadoune, I.; Maazaz, A.; Ménétrier, M.; Delmas, C. On the $Na_xNi_{0.6}Co_{0.4}O_2$ System: Physical and Electrochemical Studies. *J. Solid State Chem.* **1996**, *122*, 111−117.

(11) Komaba, S.; Nakayama, T.; Ogata, A.; Shimizu, T.; Takei, C.; Takada, S.; Hokura, A.; Nakai, I. Electrochemically Reversible Sodium Intercalation of Layered $NaNi_{0.5}Mn_{0.5}O_2$ and $NaCrO_2$. *ECS Trans.* **2008**, *16*, 43−55.

(12) Ma, X.; Chen, H.; Ceder, G. Electrochemical Properties of Monoclinic $NaMnO_2$. *J. Electrochem. Soc.* **2011**, *158*, A1307−A1312.

(13) Komaba, S.; Yabuuchi, N.; Nakayama, T.; Ogata, A.; Ishikawa, T.; Nakai, I. Study on the Reversible Electrode Reaction of $Na_{1−x}Ni_{0.5}Mn_{0.5}O_2$ for a Rechargeable Sodium-Ion Battery. *Inorg. Chem.* **2012**, *51*, 6211−6220.

(14) Yoncheva, M.; Stoyanova, R.; Zhecheva, E.; Kuzmanova, E.; Sendova-Vassileva, M.; Nihtianova, D.; Carlier, D.; Guignard, M.; Delmas, C. Structure and Reversible Lithium Intercalation in a New P'3-phase: $Na_{2/3}Mn_{1−y}Fe_yO_2$ (y = 0, 1/3, 2/3). *J. Mater. Chem.* **2012**, *22*, 23418−23427.

(15) Yoshida, H.; Yabuuchi, N.; Komaba, S. $NaFe_{0.5}Co_{0.5}O_2$ as High Energy and Power Positive Electrode for Na-ion Batteries. *Electrochem. Commun.* **2013**, *34*, 60−63.

(16) Zhou, Y.; Ding, J.; Nam, K.; Yu, X.; Bak, S.; Hu, E.; Liu, J.; Bai, J.; Li, H.; Fu, Z.; Yang, X. Phase Transition Behavior of $NaCrO_2$ During Sodium Extraction Studied by Synchrotron-Based X-ray Diffraction and Absorption Spectroscopy. *J. Mater. Chem. A* **2013**, *1*, 11130−11134.

(17) Vassilaras, P.; Ma, X.; Li, X.; Ceder, G. Electrochemical Properties of Monoclinic $NaNiO_2$. *J. Electrochem. Soc.* **2013**, *160*, A207−A211.

(18) Vassilaras, P.; Toumar, A. J.; Ceder, G. Electrochemical Properties of $NaNi_{1/3}Co_{1/3}Fe_{1/3}O_2$ as a Cathode Material for Na-Ion Batteries. *Electrochem. Commun.* **2014**, *38*, 79−81.

(19) Lee, E.; Sahgong, S.; Johnson, C. S.; Kim, Y. Comparative Electrochemical Sodium Insertion/Extraction Behavior in Layered Na_xVS_2 and Na_xTiS_2. *Electrochim. Acta* **2014**, *143*, 272−277.

(20) Han, M. H.; Gonzalo, E.; Casas-Cabanas, M.; Rojo, T. Structural Evolution and Electrochemistry of Monoclinic $NaNiO_2$ upon the First Cycling Process. *J. Power Sources* **2014**, *258*, 266−271.

(21) Ma, J.; Bo, S.; Wu, L.; Zhu, Y.; Grey, C. P.; Khalifah, P. G. Ordered and Disordered Polymorphs of $Na(Ni_{2/3}Sb_{1/3})O_2$: Honeycomb-Ordered Cathodes for Na-Ion Batteries. *Chem. Mater.* **2015**, *27*, 2387−2399.

(22) Wu, D.; Li, X.; Xu, B.; Twu, N.; Liu, L.; Ceder, G. $NaTiO_2$: A Layered Anode Material for Sodium-Ion Batteries. *Energy Environ. Sci.* **2015**, *8*, 195−202.

(23) Qi, Y.; Xu, Q.; Van der Ven, A. Chemically Induced Crack Instability When Electrodes Fracture. *J. Electrochem. Soc.* **2012**, *159*, A1838−A1843.

(24) Woodford, W. H.; Chiang, Y.-M.; Carter, W. C. Electrochemical Shock in Ion-Intercalation Materials with Limited Solid-Solubility. *J. Electrochem. Soc.* **2013**, *160*, A1286−A1292.

(25) Chang, D.; Huo, H.; Johnston, K. E.; Ménétrier, M.; Monconduit, L.; Grey, C. P.; Van der Ven, A. Elucidating the Origins of Phase Transformation Hysteresis During Electrochemical Cycling of Li-Sb Electrodes. *J. Mater. Chem. A* **2015**, *3*, 18928−18943.

(26) Kim, S.; Ma, X.; Ong, S. P.; Ceder, G. A Comparison of Destabilization Mechanisms of the Layered Na_xMO_2 and Li_xMO_2 Compounds upon Alkali De-Intercalation. *Phys. Chem. Chem. Phys.* **2012**, *14*, 15571−15578.

(27) Didier, C.; Guignard, M.; Suchomel, M. R.; Carlier, D.; Darriet, J.; Delmas, C. Thermally and Electrochemically Driven Topotactical Transformations in Sodium Layered Oxides Na_xVO_2. *Chem. Mater.* **2016**, *28*, 1462−1471.

(28) Carlier, D.; Blangero, M.; Ménétrier, M.; Pollet, P.; Doumerc, J.; Delmas, C. Sodium Ion Mobility in Na_xCoO_2 (0.6 < x < 0.75) Cobaltites Studied by ^{23}Na MAS NMR. *Inorg. Chem.* **2009**, *48*, 7018−7025. PMID: 19419150.

(29) Li, X.; Ma, X.; Su, D.; Liu, L.; Chisnell, R.; Ong, S. P.; Chen, H.; Toumar, A.; Idrobo, J.; Lei, Y.; Bai, J.; Wang, F.; Lynn, J. W.; Lee, Y. S.; Ceder, G. Direct Visualization of the Jahn-Teller Effect Coupled to Na Ordering in $Na_{5/8}MnO_2$. *Nat. Mater.* **2014**, *13*, 586−592.

(30) Silbernagel, B. G.; Whittingham, M. S. The Physical Properties of the Na_xTiS_2 Intercalation Compounds: A Synthetic and NMR Study. *Mater. Res. Bull.* **1976**, *11*, 29−36.

(31) Winn, D. A.; Shemilt, J. M.; Steele, B. C. H. Titanium Disulphide: A Solid Solution Electrode for Sodium and Lithium. *Mater. Res. Bull.* **1976**, *11*, 559−566.

(32) Hibma, T. Ordering of the Alkali-Ions in Na_xTiS_2 and Li_xTiS_2. *Physica B+C* **1980**, *99B*, 136−140.

(33) Van Der Ven, A.; Thomas, J. C.; Xu, Q.; Swoboda, B.; Morgan, D. Nondilute Diffusion from First Principles: Li Diffusion in Li_xTiS_2. *Phys. Rev. B: Condens. Matter Mater. Phys.* **2008**, *78*, 1−12.

(34) Emly, A.; Van der Ven, A. Mg Intercalation in Layered and Spinel Host Crystal Structures for Mg Batteries. *Inorg. Chem.* **2015**, *54*, 4394−4402.

(35) Kanamori, J. Infinite Series of Ground States of the Ising Model on the Honeycomb Lattice. *J. Phys. Soc. Jpn.* **1984**, *53*, 250−260.

(36) Wang, Y.; Ding, Y.; Ni, J. Ground-State Phase Diagram of Na_xCoO_2: Correlation of Na Ordering with CoO_2 Stacking Sequences. *J. Phys.: Condens. Matter* **2009**, *21*, 035401.

(37) Momma, K.; Izumi, F. VESTA 3 for Three-Dimensional Visualization of Crystal, Volumetric and Morphology Data. *J. Appl. Crystallogr.* **2011**, *44*, 1272−1276.

(38) Van der Ven, A.; Aydinol, M. K.; Ceder, G.; Kresse, G.; Hafner, J. First-Principles Investigation of Phase Stability in Li_xCoO_2. *Phys. Rev. B: Condens. Matter Mater. Phys.* **1998**, *58*, 2975−2987.

(39) Chen, Z.; Lu, Z.; Dahn, J. R. Staging Phase Transitions in Li_xCoO_2. *J. Electrochem. Soc.* **2002**, *149*, A1604−A1609.

(40) Kresse, G.; Furthmüller, J. Efficiency of ab-initio Total Energy Calculations for Metals and Semiconductors Using a Plane-Wave Basis Set. *Comput. Mater. Sci.* **1996**, *6*, 15−50.

(41) Kresse, G.; Furthmüller, J. Efficient Iterative Schemes for ab initio Total-Energy Calculations Using a Plane-Wave Basis Set. *Phys. Rev. B: Condens. Matter Mater. Phys.* **1996**, *54*, 11169−11186.

(42) Kresse, G.; Hafner, J. Norm-Conserving and Ultrasoft Pseudopotentials for First-Row and Transition Elements. *J. Phys.: Condens. Matter* **1994**, *6*, 8245−8257.

(43) Kresse, G.; Joubert, D. From Ultrasoft Pseudopotentials to the Projector Augmented-Wave Method. *Phys. Rev. B: Condens. Matter Mater. Phys.* **1999**, *59*, 1758−1775.

(44) Klimeš, J.; Bowler, D. R.; Michaelides, A. A Critical Assessment of Theoretical Methods for Finding Reaction Pathways and Transition States of Surface Processes. *J. Phys.: Condens. Matter* **2010**, *22*, 074203.

(45) Dion, M.; Rydberg, H.; Schröder, E.; Langreth, D. C.; Lundqvist, B. I. Van der Waals Density Functional for General Geometries. *Phys. Rev. Lett.* **2004**, *92*, 246401−1.

(46) Román-Pérez, G.; Soler, J. M. Efficient Implementation of a Van der Waals Density Functional: Application to Double-Wall Carbon Nanotubes. *Phys. Rev. Lett.* **2009**, *103*, 096102.

(47) Klimeš, J.; Bowler, D. R.; Michaelides, A. Van der Waals Density Functionals Applied to Solids. *Phys. Rev. B: Condens. Matter Mater. Phys.* **2011**, *83*, 195131.

(48) Ceder, G. A Derivation of the Ising Model for the Computation of Phase Diagrams. *Comput. Mater. Sci.* **1993**, *1*, 144−150.

(49) Sanchez, J. M.; Ducastelle, F.; Gratias, D. Generalized Cluster Description of Multicomponent Systems. *Phys. A* **1984**, *128*, 334−350.

(50) deFontaine, D. Cluster Approach to Order-Disorder Transformations in Alloys. *Solid State Phys.* **1994**, *47*, 33−176.

(51) CASM, v0.1.0 (2015). Available from https://github.com/prisms-center/CASMcode. DOI: 10.5281/zenodo.31216.

(52) Thomas, J. C.; Van der Ven, A. Finite-Temperature Properties of Strongly Anharmonic and Mechanically Unstable Crystal Phases from First Principles. *Phys. Rev. B: Condens. Matter Mater. Phys.* **2013**, *88*, 214111.

(53) Puchala, B.; Van Der Ven, A. Thermodynamics of the Zr-O System from First-Principles Calculations. *Phys. Rev. B: Condens. Matter Mater. Phys.* **2013**, *88*, 094108.

(54) Van der Ven, A.; Thomas, J. C.; Xu, Q.; Bhattacharya, J. Linking the Electronic Structure of Solids to Their Thermodynamic and Kinetic Properties. *Math. Comput. Simul.* **2010**, *80*, 1393−1410.

(55) Hart, G. L. W.; Blum, V.; Walorski, M. J.; Zunger, A. Evolutionary Approach for Determining First-Principles Hamiltonians. *Nat. Mater.* **2005**, *4*, 391−394.

(56) Dalton, A. S.; Belak, A. A.; Van der Ven, A. Thermodynamics of Lithium in $TiO_2(B)$ from First Principles. *Chem. Mater.* **2012**, *24*, 1568−1574.

(57) Rouxel, J.; Danot, M.; Bichon, J. LesComposés Intercalaires Na_xTiS_2. Étude Structurale Générale des Phases Na_xTiS_2 et K_xTiS_2. *Bull. Soc. Chim. Fr.* **1971**, *53*, 3930−3935.

(58) Toumar, A. J.; Ong, S. P.; Richards, W. D.; Dacek, S.; Ceder, G. Vacancy Ordering in O3-Type Layered Metal Oxide Sodium-Ion Battery Cathodes. *Phys. Rev. Applied* **2015**, *4*, 1−9.

(59) Reimers, J. N.; Dahn, J. R. Electrochemical and In Situ X-Ray Diffraction Studies of Lithium Intercalation in Li_xCoO_2. *J. Electrochem. Soc.* **1992**, *139*, 2091−2097.

(60) Lee, E.; Lee, W. C.; Asl, N. M.; Kim, D.; Slater, M.; Johnson, C.; Kim, Y. Reversible $NaVS_2$ (De)Intercalation Cathode for Na-Ion Batteries. *ECS Electrochem. Lett.* **2012**, *1*, A71−A73.

(61) Radin, M. D.; Van der Ven, A. The Stability of Prismatic and Octahedral Coordination in Layered Oxides and Sulfides Intercalated with Alkali and Alkaline-Earth Metals. *Chem. Mater.* **2016**, DOI: 10.1021/acs.chemmater.6b03454.

(62) Gabrisch, H.; Yazami, R.; Fultz, B. The Character of Dislocations in $LiCoO_2$. *Electrochem. Solid-State Lett.* **2002**, *5*, A111−A114.